RESEARCH ARTICLE

Morphological Characterization of Porous Anodic Alumina Membranes Prepared in Sulphuric, Oxalic, Chromic and Phosphoric Acids

P. Ramana Reddy[1,2,], Ajith K.M.[2], N.K. Udayashankar[2]*

Porous Anodic Alumina membranes (PAAM) have a significant role in nanoscale devices due to their easily tunable structural aspects and variety of applications in nanotechnology. The variable process parameters in the synthesis of PAAM were anodization potential, temperature, duration and nature of electrolyte concentration. Pores of different sizes and geometry were obtained by varying these anodization parameters. In the present work, PAAM were prepared in 0.3 M of sulphuric, oxalic, chromic and phosphoric acids as electrolyte and with anodization potentials (20, 40, 50 and 90 V) at a temperature of 8 °C. Field-emission Scanning Electron Microscopy investigations confirm the pore formation in PAAM layers. Pore ordering was calculated using the Fast Fourier transform (FFT) of top view SEM micrographs. Pore arrangement analysis of PAAM was studied using Image-J and WSxM software. Morphological features of PAAM such as pore diameter, interpore distance, porosity and pore density were calculated in all electrolytes. Results show that, PAAM formed in oxalic acid having high regularity ratio and circularity compared with other cases.

Introduction

Anodization of aluminium is a simple, low cost and electro-chemical process that results formation of porous anodic alumina membranes (PAAM) of different morphology by varying process parameters such as anodization potential [**1**], duration [**2,3**], temperature [**4-6**] and nature of electrolyte concentration [**7-9**]. Many research groups have intensively working on optimization of synthesis part of PAAM, having applications in electronics and photonics [**10**], energy storage [**11**], sensors [**12**], drug delivery [**13**] and to obtain nanotubular materials [**14**]. To reduce high current densities results from oxide dissolution, most of the researchers have studied anodization of aluminium at low temperatures (0 - 8° C) [**15-16**]. This gives slow oxidation growth rate [**17**], which requires long anodization duration for the preparation of PAAM. The structural aspects of PAAM such as oxide growth rate and barrier layer thickness strongly depends on anodization potential was some of the researchers already studied [**18**]. Both pore diameter and interpore distance increases linearly with increasing anodization potential [**19**], electrolyte concentration [**20**] were already reported.

Mask fabrications [**21**], lithography techniques [**22,23**] and plasma treatments [**24**] are generally used methods to prepare PAAM with better pore arrangement and hexagonal array structure. Some of the drawbacks using these methods are: time-consuming, high cost and scaling limitations. Two-step anodization process is the simplest way to prepare highly ordered PAAM structures [**25-26**]. After formation of the first step layer, subsequently removed and followed by second step with same anodizing conditions. Chosen of anodizing conditions are critical parameters for achieving PAAM with highly uniform ordered porous structure [**27**]. Aluminium grain sizes, impurity concentrations and the local crystal orientation of Al play a major role in fabrication of PAAM [**28**]. Al substrate is having significant influence on the formation of better pore arrangement and highly ordered regularity of the pores [**29**]. In particular, optimization of process parameters and electrolyte concentration in oxalic acid was already studied [**30,20**]. The main aim of the present work is to fabricate PAAM in different electrolytes and to study the circularity and degree of pore order in sulphuric, oxalic chromic and phosphoric acids. Herein, we demonstrated a detailed structural characterization of PAAM fabricated in 0.3 M of sulphuric, oxalic, chromic and phosphoric acid as electrolytes. Mainly the structural aspects like pore

[1]Department of Physics, Vignan's Foundation for Science, Technology and Research, Vadlamudi, Guntur 522213, Andhra Pradesh, India
[2]Department of Physics, National Institute of Technology Karnataka, Surathkal, Mangalore 575025, India

*Corresponding author:
E-mail: ramana.nitk@gmail.com

DOI: 10.5185/aml.2021.15704

diameter, interpore distance, porosity, pore density, circularity and regularity ratio of pores were analysed in all electrolytes. The present work highlights a complete morphological characterization of PAAM in sulphuric, oxalic, chromic and phosphoric acids.

Experimental

Initially, high purity (99.998 %, 0.3 mm thickness, Alfa Easer) annealed Al foil was cut into samples (2.5 x 1 cm) with working area of 1 cm^2. To remove the prevalent stress and strain and re-crystallize the surface along any particular direction, the Al foils were annealed at 500 °C for 5 h [**2**]. Before anodization, foils were decreased in C_2H_5OH, followed by distilled water and electrochemically smoothed in a mixture of per chloric acid and ethanol (1:4 Volume ratio) at voltage of 15 V, at 10 °C for 1min [**31,32**]. Then the samples were anodized in 0.3 M of sulphuric, oxalic, chromic and phosphoric acids at 20, 40, 50 and 90 V respectively, with anodization duration of 12 h at 8 °C. After the anodization formed oxide layer was chemically removed from the Al metal surface using etchant solution having 6wt% H_3PO_4 and 1.8 wt% H_2CrO_4 at 60 °C for 2h [**33**]. After removal, the sample was anodized again with same conditions for 12 h. The determination of pore diameter, interpore distance, pore density, porosity and regularity ratio was performed by image analysis of SEM micrographs of PAAM using the Image-J 1.5 (NIH, USA) and WSxM 5.70 software (Nanotech, Spain) [**34,35**]. The morphological characterization was carried out using field emission scanning electron microscope (JEOL/JSM-6380LA).

Results and discussion

Pore formation mechanism

Pore formation mechanism in PAAM was shown in the **Fig. 1**. It is generally accepted that, from the volume expansion stress model, porous layer is formed due to inward migration of O^{2-}, OH^- and outward migration of Al^{3+} ions [**36**]. After forming the oxide layer in PAAM, the volume of the aluminium being consumed is larger than the volume of the formed oxide layer. The lowest free energy resulted in the self-assembled, compact hexagonal arrays of pores. On the other hand, due to the spherical pore had the smallest surface area, PAAM has the most stable structure [**37**]. For the steady state growth of porous oxide layer, at the pore bases the incorporation of anions into the oxide layer occurs, gives a direct result of migration of electrolyte species. These migration of electrolyte species is related to migration of Al^{3+} and O^{2-}, OH^- ions between oxide/ electrolyte and metal/oxide interfaces [**38**]. Migration of electrolyte species is differs in different types of electrolytes. In case of sulphuric (sulphates), oxalic (oxalates) and phosphoric (phosphates) acids it is related to migration rate of O^{2-}, OH^- ions and in chromic acid (chromates) is related to migration rate of Al^{3+} ions [**18**]. May be this is the reason in case of chromic acid oxide layer is forming more than one layer compared with sulphuric, oxalic and phosphoric acids and it was also shown in the **Fig. 1**.

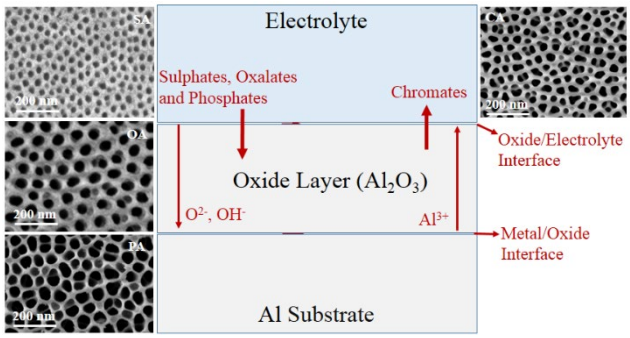

Fig. 1. Shows the growth mechanism of PAAM obtained in different electrolytes.

Morphological aspects of PAAM

In order to perform a detailed study of morphological aspects of PAAM, alumina membranes were prepared in 0.3 M of sulphuric, oxalic, chromic and phosphoric acids with anodization potential of 20, 40, 50 and 90 V respectively, about a temperature of 8°C. SEM micrographs (**Fig. 2 (a,b,c,d)**), 2D Fast Fourier Transform (FFT) images (**Fig. 2 (e,f,g,h)**) and corresponding average profiles (**Fig. 2 (i,j,k,l)**) of the FFT radius of PAAM were shown in the **Fig. 2** in all four cases . From the **Fig. 2**, it was observed that PAAM were exhibited uniform array of pores in three

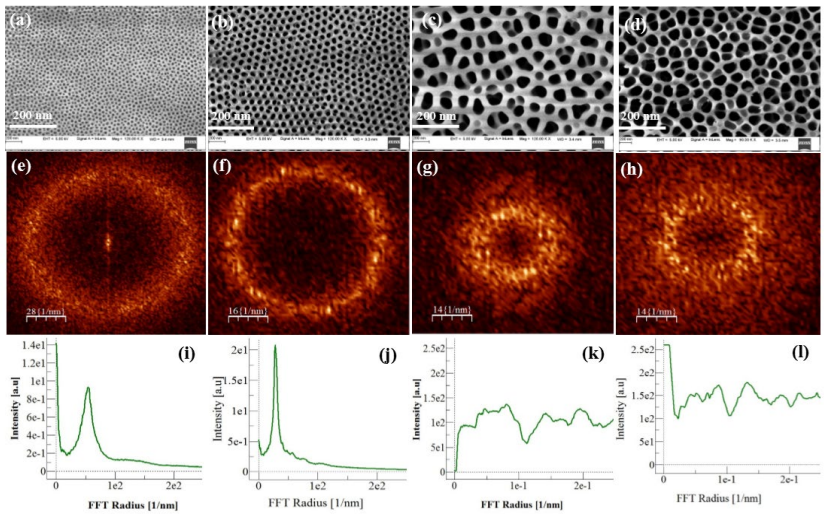

Fig. 2. SEM top views with 2DFFT and average profiles of the FFT radius of PAAM formed in 0.3 M of sulphuric (**a, e, i**), oxalic (**b, f, j**), chromic (**c, g, k**) and phosphoric (**d, h, l**) respectively.

cases. But in case of oxalic acid highly ordered pores with hexagonal structure was observed. This is due to less number of anionic incorporation in oxalic acid compared with other acids [**39**]. This anionic content plays a major role in the steady-state growth of oxide layer during the anodization process. Image-J software was used to identify all nanopores in SEM image. Circularity, area and center of mass coordinates were measured for each pore in this step. The average pore diameter, interpore distance, porosity and pore density of PAAM were calculated using the formulae from the dedicated executable publication [**40,41**]. Structural aspects such as pore diameter (**Fig. 3(a)**), interpore distance (**Fig. 3(b)**), pore density (**Fig. 3(c)**) and porosity (**Fig. 3(d)**) versus four acids were shown in the **Fig. 3**. The average pore diameter and interpore distance in sulphuric, oxalic, chromic and phosphoric acids were observed as 32, 62, 128 and 226 nm and 62, 128, 254 and 450 nm respectively. It was noticed that highest porosity in case of sulphuric acid and pore density in case of oxalic acid. **Fig. 4** illustrate the circularity (**Fig. 4(a)**) and regularity ratio (RR- **Fig. 4(b)**) of PAAM versus four acids. Pore shape was calculated using circularity coefficient [**42**] and in case of oxalic acid it was nearly equal to one compared with other acids. This is because of highly ordered hexagonal porous structure was formed in oxalic acid. This is due to highly ordered uniform porous structure is formed in oxalic acid case and it was confirmed from SEM image (**Fig. 2**). To obtain quantitative evolution of hexagonal arrangement of pores in PAAM, RR was estimated using WSxM software [**43**] and in oxalic acid case it is high value, compared with other acids. This is due to poor pore ordering in sulphuric and phosphoric acids compared with oxalic acid. It was confirmed by blurred ring on FFT profiles, intensity of radial average profile is also low in sulphuric and phosphoric acids. During the steady state growth rate of oxide formation in PAAM, oxide dissolution rate is more in oxalic acid compared with other acids. The structural aspects of PAAM data in four cases were noticed in **Table 1**.

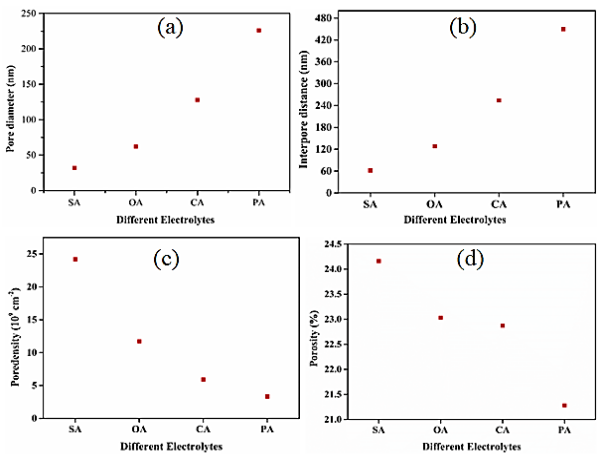

Fig. 3. Effect of pore diameter (**Fig. 3a**), interpore distance (**Fig. 3b**), pore density (**Fig. 3c**) and porosity (**Fig. 3d**) of PAAM on different electrolytes.

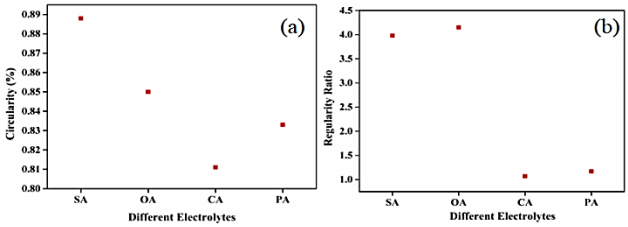

Fig. 4. Effect of circularity (**Fig. 4a**) and regularity ratio (**Fig. 4b**) as a function of different electrolytes.

Table. 1. Structural aspects of PAAM obtained in different electrolytes.

Electrolyte Name	Pore Diameter (nm)	Interpore distance (nm)	Pore density (X 10^9 cm^{-2})	Porosity (%)	Regularity ratio	Circularity (%)
Sulphuric acid	32	62	24.19	24.16	3.98	0.888
Oxalic acid	62	128	11.72	23.03	4.15	0.85
Chromic acid	128	254	5.91	22.87	1.07	0.811
Phosphoric acid	226	450	3.33	21.28	1.17	0.833

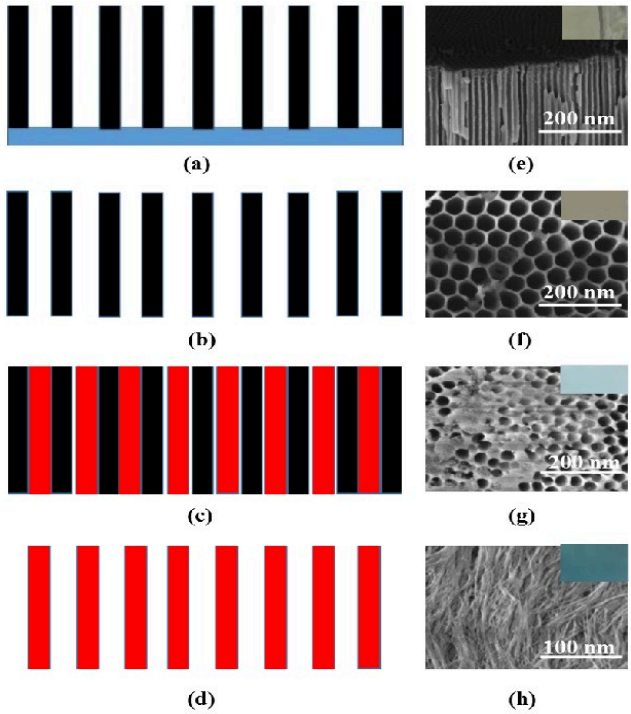

Fig. 5. Schematic of synthesis of Cu nanowires into the pores of PAAM. **(a)** PAAM with highly ordered pores, **(b)** Free standing PAAM film, **(c)** Electroless deposition of copper nitrate solution into the pores of PAAM and **(d)** Formation of Cu nanowires. The corresponding FE-SEM images and variation of colour (inset) of the sample for each step (**e, f, g** and **h**) of fabrication of Cu nanowires.

Synthesis of Cu nanowire

In-depth analysis of structural aspects of PAAM, it was noticed that highly ordered uniform array of pores were observed in 0.3 M of oxalic acid at 40 V. This PAAM is used to fabricate copper nanowire array via electroless deposition process which is shown in **Fig. 5**. After pore widening of PAAM for 30 min in 5 Wt% H_3PO_4, it was found that the pore diameter was ~ 68 nm with thickness ~ 110 mm. This is

due to decrease in barrier layer thickness of PAAM with increasing the etching time [**44**]. Removal of barrier layer using saturated copper chloride solution is shown in the **Fig. 5(b)**. Then 0.5 M of copper nitrate solution was injected into the pores of free-standing PAAM and dried at room temperature (**Fig. 5(c)**) for 2h. Finally copper nanowires were obtained inside the pores of PAAM after annealing the sample at 60 ºC for 4h (**Fig. 5(d)**). During the annealing time, copper nitrate solution undergo thermal decomposition in the presence of excess of oxygen leading to the formation of copper nanowires. The conversion of the formed copper oxide into the pure copper nanowires after 4h continuous annealing was confirmed from the colour change (**Fig. 5(h)**) of the sample and also from the EDX analysis. The corresponding FESEM images of PAAM and variation of colour of the sample (Inset) for each step was illustrated in **Fig. 5(e) – Fig. 5(h)** respectively. **Fig. 6** shows the typical FE-SEM images of free standing Cu nanowires fabricated into the pores of PAAM by electroless deposition method [**45**]. Cu nanowires grown were highly homogeneous in shape, continuous and uniform throughout the surface of the membrane (**Fig. 6(a)**). Higher magnified Cu nanowire (**Fig. 6(b)**) array reveals that nanowires were randomly oriented on the pores of PAAM and tips of the nanowires aggregated into clumps. The cross-section image of PAAM is shown in **Fig. 6(c)**. Inset images illustrate the variation of pore wall before and after deposition of Cu nanowires. It was observed that after deposition of Cu nanowires pore wall crushes near to the surface of PAAM. The EDX spectra showed in the **Fig. 6(d)** confirms the existence of Cu. The dimensions of Cu nanowires are consistent with the average value of pore diameter of PAAM. It may be noted that such copper nanowires have wide ranging applications in gas sensing, field emission and photovoltaic devices, light emitting diodes and thin film solar cells [**46**].

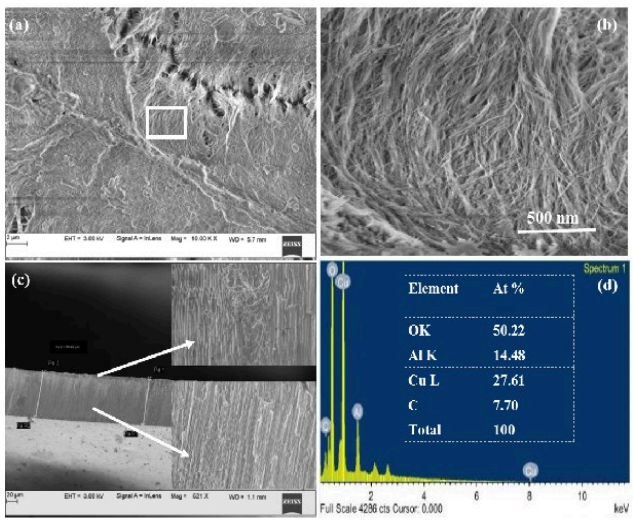

Fig. 6. (a) FE-SEM images of copper nanowires grown inside the pores of PAAM, **(b)** Higher magnified image of randomly oriented Cu nanowires, **(c)** Variation of cross-sectional image PAAM before and after growth of Cu nanowires and **(d)** EDX spectra of Cu nanowires.

Conclusions

In summary, PAAM were prepared in 0.3 M of sulphuric, oxalic, chromic and phosphoric acid as electrolytes and with anodization potentials (20, 40, 50 and 90 V) at a temperature of 8 °C. Field-emission Scanning Electron Microscopy investigations confirm the pore formation in PAAM layers. Pore ordering was calculated using the Fast Fourier transform (FFT) of top view SEM micrographs. Pore arrangement analysis of PAAM was studied using Image-J and WSxM software. Morphological features of PAAM such as pore diameter, interpore distance, porosity and pore density were calculated in all electrolytes. Results show that, PAAM formed in oxalic acid having high regularity ratio and circularity compared with other cases. After pore widening duration of PAAM for 30 min, pore diameter changes from 62 nm to 68 nm. Copper nanowires were grown into the pores of PAAM by electroless deposition method. Cu nanowires were randomly oriented through the surface of the membrane and tips of the nanowires aggregate into clumps.

Acknowledgment

The one of the author P. Ramana Reddy wishes to acknowledge MHRD for their financial support throughout the research work.

Author's contribution

Author A: Designed and performed the experiments, analyzed data and co-write the paper. Author B and C: Conceived of the study and acquisition data, participated in its design and coordination and helped to draft the manuscript. All authors have participated in (a) conception and design, or analysis and interpretation of the data; (b) drafting the article or revising it critically for important intellectual content; and (c) approval of the final version. All authors read and approved the final manuscript.

Keywords

Porous anodic alumina membranes, two-step anodization, circularity, pore diameter, porosity and pore density

Received: 25 May 2021
Revised: 16 July 2021
Accepted: 16 July 2021

References

1. Bai, A.; Hu, C.C.; Yang, Y.F.; Lin, C.C.; *Electrochimica Acta,* **2008**, *53,* 2258.
2. Reddy, P.R.; Ajith, K.M.; Udayashankar, N.K.; *Journal of Materials Science: Materials in Electronics,* **2016**, *27,* 5331.
3. Bruera, F.A.; Kramer, G.R.; Vera, M.L.; Ares, A.E.; *Coatings,* **2019**, *9,* 115.
4. Stempniowski, W.J.; Bojar, Z.; *Surface and Coatings Technology,* **2011**, *206,* 265.
5. Zaraska, L.; Stempniowski, W.J.; Ciepiela, E.; Sulka, G.D.; *Thin Solid Films,* **2013**, *534,* 155.
6. Bruera, F.A.; Kramer, G.R.; Vera, M.L.; Ares, A.E.; *Surfaces and Interfaces,* **2020**, *18,* 100448.
7. Stempniowski, W.J.; Moneta, M.; Norek, M.; Michalska-Domanska, M.; Scarpellini, A.; Salerno, M.; *Electrochimica Acta,* **2016**, *211,* 453.
8. Reddy, P.R.; Ajith, K.M.; Udayashankar, N.K.; *Ceramics International,* **2016**, *42,* 17806.
9. Bruera, F.A.; Kramer, G.R.; Vera, M.L.; Ares, A.E.; *Coatings,* **2021**, *11,* 309.

10. Cheng, C.; Electro-Chemo-Mechanics of Anodic Porous Alumina Nano-Honeycombs: Self-Ordered Growth and Actuation, Springer, **2015**.
11. Jani, A.M.M.; Losic, D.; Voelcker, N.H.; *Progress in Materials Science,* **2013**, *58,* 636.
12. Santos, A.; Balderrama, V.S.; Alba, M.; Formentín, P.; Ferré-Borrull, J.; Pallarès, J.; Marsal, L.F.; *Advanced Materials,* **2012**, *24,* 1050.
13. Losic, D.; Simovic, S.; *Expert Opinion on Drug Delivery,* **2009**, *6,* 1363.
14. St¸epniowski, W.J.; Salerno, M.; *Manufacturing Nanostructures,* **2014**, 321.
15. Sulka, G.D.; Stempniowski, W.J.; *Electrochimica Acta,* **2009**, *54,* 3683.
16. Reddy, P.R.; Ajith, K.M.; Udayashankar, N.K.; *Applied Physics A,* **2018**, *124,* 765.
17. Jessensky, O.; Müller, F.; Gösele, U.; *Applied Physics Letters,* **1998**, *72,* 1173.
18. Alkire, R.C.; Gogotsi, Y.; Simon, P.; Nanostructured Materials in Electrochemistry, John Wiley & Sons, **2008**.
19. Sulka, G.D.; Parko\la, K.G.; *Thin Solid Films,* **2006**, *515,* 338.
20. Ramana Reddy, P.; Ajith, K.M.; Udayashankar, N.K.; *Materials Science in Semiconductor Processing,* **2020**, *106,* 104755.
21. Masuda, H.; Asoh, H.; Watanabe, M.; Nishio, K.; Nakao, M.; Tamamura, T.; *Advanced Materials,* **2001**, *13,* 189.
22. Lee, W.; Ji, R.; Ross, C.A.; Gösele, U.; Nielsch, K.; *Small,* **2006**, *2,* 978.
23. Montero Moreno, J.M.; Waleczek, M.; Martens, S.; Zierold, R.; Görlitz, D.; Martínez, V.V.; Prida, V.M.; Nielsch, K.; *Advanced Functional Materials,* **2014**, *24,* 1857.
24. Oshima, H.; Kikuchi, H.; Nakao, H.; Itoh, K.; Kamimura, T.; Morikawa, T.; Matsumoto, K.; Umada, T.; Tamura, H.; Nishio, K.; *Applied Physics Letters,* **2007**, *91,* 022508.
25. Reddy, P.R.; A.K.M.; Udayashankar, N.K.; *Advanced Materials Letters,* **2016**, *7,* 398.
26. Prida, V.M.; Vega, V.; García, J.; Iglesias, L.; Hernando, B.; Minguez-Bacho, I.; Magnetic Nano-and Microwires, Elsevier, **2015**, pp.3-39.
27. Chi, C.S.; Lee, J.H.; Kim, I.; Oh, H.J.; *Journal of Materials Science & Technology,* **2015**, *31,* 751.
28. Rashidi, F.; Masuda, T.; Asoh, H.; Ono, S.; *Surface and Interface Analysis,* **2013**, *45,* 1490.
29. Abd-Elnaiem, A.M.; Mebed, A.M.; Gaber, A.; Abdel-Rahim, M.A.; *Journal of Alloys and Compounds,* **2016**, *659,* 270.
30. Stempniowski, W.J.; Zasada, D.; Bojar, Z.; *Surface and Coatings Technology,* **2011**, *206,* 1416.
31. Reddy, P.R.; Ajith, K.M.; Udayashankar, N.K.; *Materials Today: Proceedings,* **2019**, *19,* 2633.
32. Bruera, F.A.; Kramer, G.R.; Vera, M.L.; Ares, A.E.; *Superlattices and Microstructures,* **2019**, *130,* 103.
33. Stempniowski, W.J.; Moneta, M.; Norek, M.; Michalska-Domanska, M.; Scarpellini, A.; Salerno, M.; *Electrochimica Acta,* **2016**, *211,* 453.
34. Vega, V.; García, J.; Montero-Moreno, J.M.; Hernando, B.; Bachmann, J.; Prida, V.M.; Nielsch, K.; *ACS Applied Materials & Interfaces,* **2015**, *7,* 28682.
35. Stempniowski, W.J.; Doma. ń. ska M.; Norek, M.; Czujko, T.; *Materials Letters,* **2014**, *117,* 69.
36. Shimizu, B.K.; Kobayashi, K.; Thompson, G.E.; Wood, G.C.; *Philosophical Magazine B,* **1991**, *64,* 345.
37. Yang, Z.B.; Hu, J.C.; Li, K.Q.; Zhang, S.Y.; Fan, Q.H.; Liu, S.A.; in IOP Conference Series: Materials Science and Engineering IOP Publishing, **2017**, p. 012003.
38. Searson, P.C.; Moffat, T.P.; *Critical Reviews in Surface Chemistry,* **1994**, *3,* 171.
39. Thompson, G. E.; Wood, G. C.; in Treatise on Materials Science and Technology, Edited by J. C. Scully (Elsevier, **1983**), pp. 205-329.
40. Stempniowski, W.J.; Nowak-St¸epniowska, A.; Bojar, Z.; *Materials Characterization,* **2013**, *78,* 79.
41. Ciepiela, E.; Zaraska, L.; Sulka, G.D.; GridSpace2/Collage Executable Paper Http://Collage. Cyfronet. Pl/Hillebrand-Grains **2011**.
42. Zaraska, L.; Stempniowski, W.J.; Sulka, G.D.; Ciepiela, E.; Jaskuła, M.; *Appl. Phys. A,* **2014**, *114,* 571.
43. Stempniowski, W. J.; Choi, J.; Yoo, H.; Doma. ń. ska M.; Chilimoniuk, P.; Czujko, T.; *Materials Letters,* **2016**, *164,* 176.
44. Suchitra, S.M.; Reddy, P.R.; Udayashankar, N. K.; *Materials Today: Proceedings,* **2016**, *3,* 2042.
45. Ren, X.; Huang, X.; Zhang, H.; He, M.; *Frontiers of Materials Science in China,* **2007**, *1,* 312.
46. Rathmell, A.R.; Bergin, S. M.; Hua, Y.L.; Li, Z.Y.; Wiley, B.J.; *Advanced Materials,* **2010**, *22,* 3558.